

# Asymptotic Eigenvalue Density of Noise Covariance Matrices

Ravishankar Menon, *Student Member, IEEE*, Peter Gerstoft, and William S. Hodgkiss, *Member, IEEE*

**Abstract**—The asymptotic eigenvalues are derived for the true noise covariance matrix (CM) and the noise sample covariance matrix (SCM) for a line array with equidistant sensors in an isotropic noise field. In this case, the CM in the frequency domain is a symmetric Toeplitz sinc matrix which has at most two distinct eigenvalues in the asymptotic limit of an infinite number of sensors. Interestingly, for line arrays with interelement spacing less than half a wavelength, the CM turns out to be rank deficient. The asymptotic eigenvalue density of the SCM is derived using random matrix theory (RMT) for all ratios of the interelement spacing to the wavelength. When the CM has two distinct eigenvalues, the eigenvalue density of the SCM separates into two distinct lobes as the number of snapshots is increased. These lobes are centered at the two distinct eigenvalues of the CM. The asymptotic results agree well with analytic solutions and simulations for arrays with a small number of sensors.

**Index Terms**—Eigenvalue density, isotropic noise, random matrix theory, sample covariance matrix.

## I. INTRODUCTION

OVER the past decade, it has been shown that cross-correlations of a diffuse field between a pair of receivers yields the Green's function between them [1], [2]. Since ambient noise is ubiquitous, the immense potential of this technique to image remote areas of the ocean and the interior of the earth using arrays of sensors and naturally occurring noise has made it a rich area of current research in seismology [3], [4] and ocean acoustics [5], [6], and structural engineering [7] among others. The use of many receivers and the random nature of the ambient noise field provides a good setting for the application of random matrix theory (RMT) [8], [9]. Here, we study the eigenvalues of noise covariance matrices from an array of sensors.

In array processing problems, the noise field often is assumed to be *isotropic*, i.e., it consists of random waves propagating towards the array from all directions. The spatial coherence func-

tion  $\Gamma$  of the noise recorded on two sensors in a 3-D isotropic noise field is [10]

$$\Gamma = \text{sinc}(2\beta) \quad (1)$$

where  $\text{sinc}(x) = \frac{\sin(\pi x)}{(\pi x)}$  and  $\beta$  is the ratio of the spacing between the sensors to the wavelength under consideration ( $\beta = \frac{f\Delta x}{c}$ , where  $f$  is the frequency,  $\Delta x$  is the spacing between the sensors, and  $c$  is the speed of wave propagation in the medium). For a linear array of  $N$  equidistant sensors, the elements of the covariance matrix  $\Sigma$  (CM) of the noise field (normalized to unit power on each sensor) are given by

$$\Sigma_{ij} = \text{sinc}(2\beta|i-j|) \quad (2)$$

which is a symmetric Toeplitz matrix. Thus, the spatial correlations are only dependent on  $\beta$  and the separation  $|i-j|$ .

With real noise data, the sample covariance matrix (SCM)  $\hat{\Sigma}$  is estimated from  $M$  i.i.d. observations of the array snapshot vector (i.e., the Fourier coefficients of the observation vector at a particular frequency)  $\psi_m$ ,  $m = \{1, \dots, M\}$  as

$$\hat{\Sigma} = \frac{1}{M} \sum_{m=1}^M \psi_m \psi_m^H \quad (3)$$

The eigenvalues of the SCM deviate from the true CM and the density of these eigenvalues

$$\hat{p}(\lambda) = \frac{1}{N} \sum_{n=1}^N \delta(\lambda - \lambda_n) \quad (4)$$

where  $\lambda_n$  are the eigenvalues of  $\hat{\Sigma}$ , are typically studied using random matrix theory (RMT), in the asymptotic limit as the array dimension and the observation dimension both grow large proportionately, i.e.,  $N, M \rightarrow \infty$ ,  $\frac{N}{M} = \nu$ , the ratio of the number of array elements to the number of snapshots. RMT also has applications in a wide variety of fields such as signal detection [11], communication via antennas [12], information theory and wireless networks [13], elastodynamics [14] and wave propagation and scattering in random media [15]–[17].

Prior work involving RMT and eigenvalue densities relevant to this article include [18], [19]. While [18] deals with estimating the true eigenvalues of the CM from the observed SCM for a few distinct sources, we focus on the asymptotic eigenvalue density of the SCM for a noise only model (i.e., no sources). Knowledge of these densities could be used in monitoring environments, i.e., a change in the density could

Manuscript received August 31, 2011; revised January 19, 2012 and March 12, 2012; accepted March 26, 2012. Date of publication April 05, 2012; date of current version June 12, 2012. The associate editor coordinating the review of this manuscript and approving it for publication was Prof. Alfred Hanssen. This work was supported by the Office of Naval Research, Grants N00014-11-1-0321 and N00014-11-1-0320.

The authors are with the Marine Physical Laboratory at the Scripps Institution of Oceanography, University of California San Diego, La Jolla, CA 92093 USA (e-mail: rmenon@ucsd.edu; pgerstoft@ucsd.edu; whodgkiss@ucsd.edu).

Color versions of one or more of the figures in this paper are available online at <http://ieeexplore.ieee.org>.

Digital Object Identifier 10.1109/TSP.2012.2193573

be interpreted as a change in the environmental conditions. The results also could be used in conjunction with [19] to identify eigenvalues corresponding to strong interferers in the environment (e.g., ships in ocean acoustics and earthquakes in seismology). In Section III-B, it is shown that the SCM for isotropic noise fields is rank deficient even when the number of snapshots is more than the number of array elements (i.e.,  $\nu \leq 1$ ). This result is certainly important to consider in applications which require the inverse of the SCM, such as adaptive beamforming.

The rest of the paper is organized as follows. A statistical model for the SCM is chosen in Section I-A, followed by a recap of known results for an uncorrelated noise SCM. Section I-C discusses preliminary details that aid in the derivation of the eigenvalues in Section II. In Section III, the asymptotic eigenvalue density of the SCM is derived using Stieltjes transforms and studied in detail for all values of  $\beta$ . The asymptotic results are compared to analytical results for finite  $N$  in Section IV and using simulations for practical values of  $N$  in Section V, followed by conclusions in Section VI.

#### A. Statistical Model for the SCM

The noise snapshot vector is modeled as a stationary, zero-mean, complex Gaussian stochastic process with covariance  $\Sigma$ , i.e.,  $\psi_m \sim \mathcal{CN}(\mathbf{0}, \Sigma)$ . Realizations of the noise SCM then can be generated from the true CM  $\Sigma$  as [18]

$$\hat{\Sigma} = \frac{1}{M} \Sigma^{\frac{1}{2}} \mathbf{X} (\Sigma^{\frac{1}{2}} \mathbf{X})^H \quad (5)$$

where  $\mathbf{X}$  is an  $N \times M$  random matrix belonging to the Gaussian unitary ensemble (GUE)<sup>1</sup> whose entries are zero-mean complex Gaussian random variables drawn from  $\mathcal{CN}(0, 1)$ , and  $\Sigma^{\frac{1}{2}}$  is a nonnegative definite square root of the true CM,  $\Sigma$ .

Here we restrict our focus to  $\nu \leq 1$ , i.e., there are at least as many snapshots as the number of array elements, because the stationarity of the environment over reasonable intervals allows for sufficient averaging (i.e., snapshot starved scenarios are not considered).

#### B. Uncorrelated Noise at $\beta = \frac{1}{2}$

At  $\beta = \frac{1}{2}$  (half-wavelength spacing) the off-diagonal terms in (2) are zero and  $\Sigma = \mathbf{I}$ . In other words, the noise is spatially uncorrelated from sensor to sensor.

The eigenvalue density of the SCM in this case, in the limit  $N, M \rightarrow \infty$  and  $\frac{N}{M} = \nu$ , is given by the Marčenko—Pastur (MP) density [20]

$$\hat{p}_{MP}(\lambda) = \begin{cases} \frac{\sqrt{(l_+ - \lambda)(\lambda - l_-)}}{2\pi\nu\lambda} & l_- < \lambda < l_+ \\ 0 & \text{otherwise} \end{cases} \quad (6)$$

where  $l_- = (1 - \sqrt{\nu})^2$  and  $l_+ = (1 + \sqrt{\nu})^2$  are the upper and lower limits of the “spreading” of the eigenvalues of the SCM around the true eigenvalue which is 1.

<sup>1</sup>The distribution of the elements in a GUE random matrix is invariant to transformations by a unitary matrix.

This holds true for multiples of the half wavelength spacing i.e.,  $\beta = \frac{q}{2}$ ,  $q \in \mathbb{N}$  and for all other values of  $\beta$ , the noise is correlated and the densities of the SCM will deviate from the simple MP density.

#### C. Preliminaries

Symmetric sinc Toeplitz matrices (henceforth referred to as sinc matrices) also arise in solutions to certain differential [21], covariance matrix tapering [22], [23], etc. In general, the eigenvalues of an infinite dimensional Toeplitz matrix constructed from absolutely summable sequences with an absolutely summable Fourier series (called Wiener class Toeplitz matrices) are related to the Fourier series of the sequence [24], [25]. Although the underlying sinc sequence in  $\Sigma$  is not absolutely summable, this result still holds, as shown in Section II.

The relation between the Fourier transform of the sinc function and the eigenvalues of the sinc matrix has been shown previously [26], [27]. The eigenvalues of the finite dimensional sinc matrix also were studied in detail in the context of discrete prolate spheroidal wave functions [21], [27] for  $\beta \leq \frac{1}{2}$  and for block Toeplitz sinc matrices in the context of asynchronous CDMA systems [28]. In Section II, we consider the asymptotic eigenvalues of the true CM  $\Sigma$  for all  $\beta \in (0, \infty)$ , as the array dimension  $N \rightarrow \infty$ .

A key to understanding the asymptotic behavior of the eigenvalues is the behavior of the Fourier transform of the sampled sinc function when it is oversampled or undersampled (see Fig. 1). Consider the infinite sequence  $\text{sinc}(2\beta n)$  where  $n \in \mathbb{Z}$ , i.e., a sampling interval of  $\Delta x$  corresponding to the interelement spacing of the line array. The Fourier transform of the continuous sinc function is a rectangular function of bandwidth  $2\beta$  (highest frequency  $\beta$ ). In order to avoid aliasing in the Fourier transform of the sampled sinc, we need  $2\beta \leq 1$ , or  $\beta \leq \frac{1}{2}$ . At the Nyquist sampling  $\beta = \frac{1}{2}$  (and at multiples of  $1/2$ ), the sinc is sampled at only its peak and zeros, and corresponds to a unit sample. As a result, the Fourier transform is 1 [see Fig. 1(c), (d)]. When  $\beta < \frac{1}{2}$ , it is oversampled and the Fourier transform is zero outside the bandwidth of the sinc [see Fig. 1(a), (b)]. When  $\beta > \frac{1}{2}$ , the sinc function is undersampled and this introduces aliasing in the Fourier space [see Fig. 1(e), (f)]. These behaviors of the Fourier transform are reflected in the eigenvalues of the CM.

#### D. Notations

Throughout this paper, matrices are represented by bold, uppercase symbols and vectors by bold, lowercase symbols. With the exception of  $\nu$ , quantities pertaining to the SCM are denoted with a carat  $\hat{\cdot}$ . In order to compare infinite dimensional matrices, a normalized rank is defined as

$$\mathcal{R}(\cdot) = \lim_{N \rightarrow \infty} \frac{\text{rank}(\cdot)}{N}. \quad (7)$$

For convenience,  $N$  is implicitly assumed even in Section II-A, although the same can be done for odd  $N$  (asymptotic result remains unchanged).

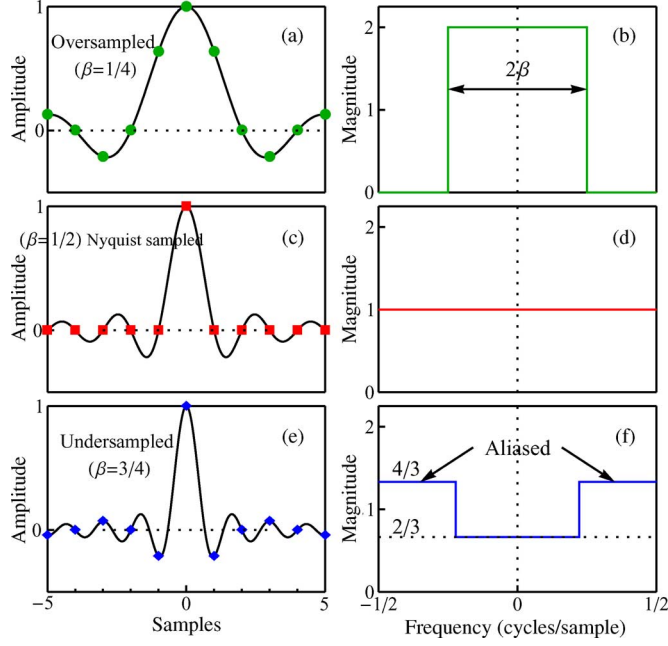


Fig. 1. Schematic showing the sinc function and its Fourier transform when  $\beta$  is (a, b) less than the Nyquist frequency (c, d) at the Nyquist frequency, i.e.,  $\beta = \frac{1}{2}$  and (e, f) greater than the Nyquist frequency.

## II. ASYMPTOTIC EIGENVALUES OF THE NOISE CM

### A. Derivation of the Eigenvalues

Let  $f_n = \text{sinc}(2\beta n)$ ,  $n \in \mathbb{Z}$  be an even sequence that is absolutely square summable, with a Fourier transform

$$\phi(\kappa) = \sum_{n=-\infty}^{\infty} f_n e^{-i2\pi\kappa n} \quad (8)$$

where  $\kappa$  is the spatial frequency.

*Proposition 1 (Asymptotic Eigenvalues of the Sinc Matrix  $\Sigma$ ):* Defining  $\lambda_k$  and  $\mathbf{u}_k$  as

$$\lambda_k = \sum_{n=-\frac{N}{2}}^{\frac{N}{2}-1} f_n e^{\frac{-i2\pi n k}{N}} \quad (9)$$

and

$$\mathbf{u}_k = \frac{1}{\sqrt{N}} \left[ 1, e^{\frac{-i2\pi k}{N}}, \dots, e^{\frac{-i2\pi k(N-1)}{N}} \right]^T \quad (10)$$

where  $k \in \{-\frac{N}{2}, \dots, \frac{N}{2} - 1\}$  is the equivalent of a discrete Fourier transform spatial frequency bin, then as  $N \rightarrow \infty$ ,  $\lambda_k$  and  $\mathbf{u}_k$  are the eigenvalues and eigenvectors of  $\Sigma$ .

*Proof:* If  $\lambda_k$  and  $\mathbf{u}_k$  are the eigenvalues and eigenvectors of  $\Sigma$ , then

$$\Sigma \mathbf{u}_k = \lambda_k \mathbf{u}_k \quad (11)$$

must hold as  $N \rightarrow \infty$ . Writing  $\Sigma$  as

$$\Sigma = \begin{bmatrix} f_0 & f_1 & \cdots & f_{N-1} \\ f_{-1} & f_0 & \cdots & f_{N-2} \\ \vdots & \vdots & \ddots & \vdots \\ f_{-N+1} & f_{-N+2} & \cdots & f_0 \end{bmatrix} \quad (12)$$

the  $j$ th element ( $j = 1, \dots, N$ ) of the vector  $\Sigma \mathbf{u}_k$  is

$$\begin{aligned} [\Sigma \mathbf{u}_k]_j &= \frac{1}{\sqrt{N}} \sum_{n=1-j}^{N-j} f_n e^{\frac{-i2\pi k(n+j-1)}{N}} \\ &= \frac{1}{\sqrt{N}} \sum_{n=1-j}^{N-j} \alpha_{jkn} \end{aligned} \quad (13)$$

where  $\alpha_{jkn} = f_n e^{\frac{-i2\pi k(n+j-1)}{N}}$  is introduced as a shorthand notation. Similarly, the  $j$ th element of the vector  $\lambda_k \mathbf{u}_k$  is

$$[\lambda_k \mathbf{u}_k]_j = \frac{1}{\sqrt{N}} \sum_{n=-\frac{N}{2}}^{\frac{N}{2}-1} \alpha_{jkn}. \quad (14)$$

Subtracting (13) from (14)

$$[\Sigma \mathbf{u}_k - \lambda_k \mathbf{u}_k]_j = \frac{1}{\sqrt{N}} \begin{cases} -\sum_{n=-\frac{N}{2}}^{-j} \alpha_{jkn} + \sum_{n=\frac{N}{2}}^{N-j} \alpha_{jkn} & j \leq \frac{N}{2} \\ -\sum_{n=1-j}^{-\frac{N}{2}-1} \alpha_{jkn} - \sum_{n=N-j+1}^{\frac{N}{2}-1} \alpha_{jkn} & j > \frac{N}{2} \end{cases} \quad (15)$$

Using the triangle inequality and reverting to the original notation, (15) results in

$$\left| [\Sigma \mathbf{u}_k - \lambda_k \mathbf{u}_k]_j \right|^2 \leq \frac{1}{N} \begin{cases} \sum_{n=-\frac{N}{2}}^{-j} |f_n|^2 + \sum_{n=\frac{N}{2}}^{N-j} |f_n|^2 & j \leq \frac{N}{2} \\ \sum_{n=1-j}^{-\frac{N}{2}-1} |f_n|^2 + \sum_{n=N-j+1}^{\frac{N}{2}-1} |f_n|^2 & j > \frac{N}{2}. \end{cases} \quad (16)$$

Taking the norm of the entire vector, and combining the terms in the first and last components, the terms in the second and penultimate components and so forth, we get

$$\begin{aligned} \|\Sigma \mathbf{u}_k - \lambda_k \mathbf{u}_k\|_2^2 &\leq \frac{1}{N} \sum_{j=1}^{\frac{N}{2}} \left( \sum_{n=-N+j}^{-j} |f_n|^2 + \sum_{n=j}^{N-j} |f_n|^2 \right) \\ &\leq \frac{2}{N} \sum_{j=1}^{\frac{N}{2}} \sum_{n=j}^{N-j} |f_n|^2 = \frac{2}{N} \sum_{j=1}^{\frac{N}{2}} \sum_{n=j}^{N-j} \text{sinc}^2(2\beta n) \\ &\leq \frac{1}{2\beta^2 N} \sum_{j=1}^{\frac{N}{2}} \sum_{n=j}^{\infty} \frac{1}{n^2}. \end{aligned} \quad (17)$$

Since the functions  $\frac{1}{x^2}$  (and  $\frac{1}{x}$ ) are strictly convex on  $(0, \infty)$ , the RHS of (17) can be simplified as

$$\begin{aligned} \sum_{j=1}^{\frac{N}{2}} \sum_{n=j}^{\infty} \frac{1}{n^2} &< \sum_{j=1}^{\frac{N}{2}} \int_{j-\frac{1}{2}}^{\infty} \frac{dx}{x^2} < \sum_{j=1}^{\frac{N}{2}} \frac{1}{j-\frac{1}{2}} \\ &< \int_{\frac{1}{2}+\epsilon}^{\frac{N}{2}+\frac{1}{2}} \frac{dy}{y-\frac{1}{2}} = \ln\left(\frac{N}{2\epsilon}\right). \end{aligned} \quad (18)$$

From (17) and (18),  $\exists \epsilon > 0$  independent of  $N$ , such that  $\ln\left(\frac{N}{2\beta^2 N}\right)$  goes to zero independent of  $k$  as  $N \rightarrow \infty$ . Hence

$$\|\Sigma \mathbf{u}_k - \lambda_k \mathbf{u}_k\|_2 \rightarrow 0 \text{ as } N \rightarrow \infty \forall k \quad (19)$$

or  $\lambda_k$  and  $\mathbf{u}_k$  are the eigenvalues and eigenvectors of  $\Sigma$ , respectively. ■

When  $N \rightarrow \infty$ , from (9) and (8),  $\lambda_k = \phi\left(\frac{k}{N}\right)$  i.e.,  $\phi(\kappa)$  sampled uniformly at  $N$  points in  $[-\frac{1}{2}, \frac{1}{2}]$ . As illustrated in Fig. 1,  $\phi(\kappa)$  only takes on one or two distinct values. Thus, the eigenvalue density  $p(\lambda)$  of  $\Sigma$  can be written succinctly as

$$p(\lambda) = \xi_1 \delta(\lambda - \Lambda_1) + \xi_2 \delta(\lambda - \Lambda_2) \quad (20)$$

where  $\Lambda_{1,2}$  are the two distinct eigenvalues and  $\xi_{1,2}$  are their multiplicity ratios defined as follows:

- 1) For  $\beta < \frac{1}{2}$  (oversampling)

$$\phi(\kappa) = \frac{1}{2\beta} \text{rect}\left(\frac{\kappa}{2\beta}\right) \quad (21)$$

where  $\text{rect}(x) = 1 \forall |x| \leq \frac{1}{2}$  and 0 elsewhere. Hence, the two distinct values of  $\lambda_k$  are

$$\Lambda_1 = \frac{1}{2\beta} \text{ and } \Lambda_2 = 0 \quad (22)$$

and the multiplicity ratios are related to the bandwidth as

$$\xi_1 = 2\beta \text{ and } \xi_2 = 1 - 2\beta. \quad (23)$$

In this case,  $\Sigma$  is rank deficient due to the zero eigenvalues.

- 2) For  $\beta = \frac{1}{2}$  (Nyquist sampling) and multiples thereof,  $\Lambda_1 = \Lambda_2 = 1$  and  $\Sigma = \mathbf{I}$ .
- 3) For  $\beta > \frac{1}{2}$  (undersampling) and not a multiple of  $1/2$ , aliasing is introduced due to the folding of the eigenvalue spectrum onto itself [see Fig. 2(b)]. As a result, both  $\Lambda_1$  and  $\Lambda_2$  are nonzero when  $\beta > \frac{1}{2}$  and  $\beta \neq \frac{q}{2}$ ,  $q \in \mathbb{N}$ , resulting in  $\Sigma$  being full rank.  $\Lambda_{1,2}$  then can be written as

$$\Lambda_1 = \frac{q+1}{2\beta} \text{ and } \Lambda_2 = \frac{q}{2\beta}, \quad (24)$$

with  $q$  such that  $q < 2\beta \leq q+1$ . The term  $\frac{q}{(2\beta)}$  accounts for the folding of the spectrum. Similarly, the multiplicity ratios are given by

$$\xi_1 = 2\beta - q \text{ and } \xi_2 = q + 1 - 2\beta. \quad (25)$$

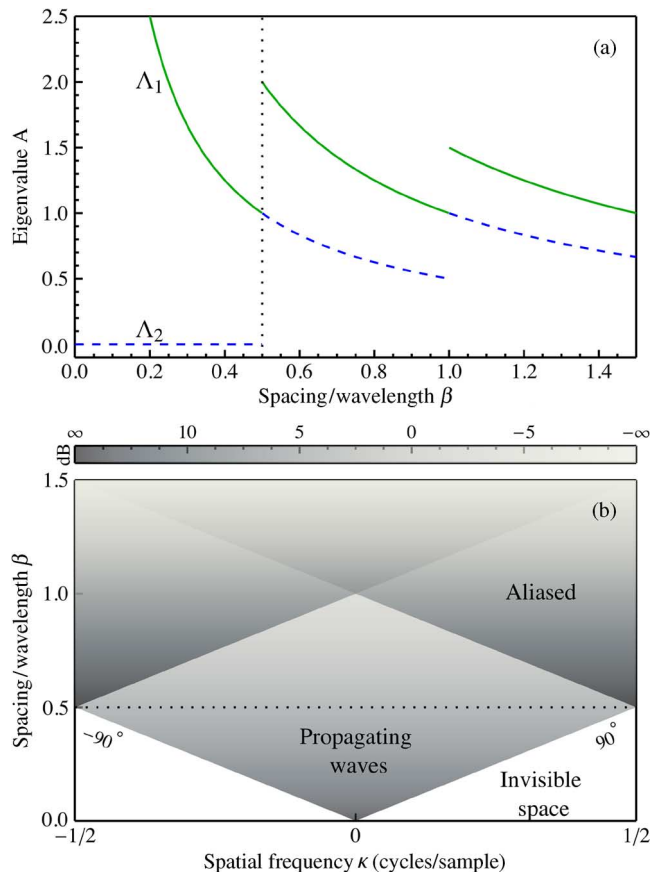


Fig. 2. (a) Distinct eigenvalues  $\Lambda_1$  (solid) and  $\Lambda_2$  (dashed) of  $\Sigma$  versus  $\beta$ , the ratio of spacing to wavelength. The dotted line marks  $\beta = \frac{1}{2}$  the half-wavelength spacing. (b) Change in eigenvalues versus spatial frequency and  $\beta$ . The invisible space and aliased regions also are marked.

### B. Physical Interpretation and Effects of Finite Arrays

For  $\beta \leq \frac{1}{2}$ , the eigenvectors (10) of the nonzero eigenvalues correspond to waves from specific angles  $\theta_\kappa$  impinging on the array

$$\theta_\kappa = \arcsin\left(\frac{\kappa}{\beta}\right). \quad (26)$$

Thus  $\theta_0 = 0$  corresponds to a wave impinging at broadside and  $\theta_{\pm\beta} = \pm\frac{\pi}{2}$  corresponds to the array end-fire direction (see Fig. 2). The zero eigenvalues  $\Lambda_2$  for  $\beta < \frac{1}{2}$  correspond to the invisible space [29, Section 3.3.2], as it does not correspond to any propagating wave [see Fig. 2(b)].

For finite  $N$  the transition between  $\Lambda_1$  and  $\Lambda_2$  becomes more gradual due to truncation effects similar to the effect observed for finite Fourier transforms and this is discussed in Section V. Approximations for the eigenvalues in the transition region for finite  $N$  are described in [21], scaled down by a factor of  $2\beta$ .

### III. ASYMPTOTIC EIGENVALUE DENSITY OF THE NOISE SCM USING RANDOM MATRIX THEORY

For the statistical assumptions made in (5), the eigenvalue density  $\hat{p}(\lambda)$  of  $\hat{\Sigma}$  converges to a probability density function

that is related to the true eigenvalue spectral density  $p(\lambda)$  of  $\Sigma$  [30].

The behavior of the eigenvalues of the SCM in the asymptotic limit, is characterized by the Stieltjes transform of its distribution [31]. In this section, we present the relevant results from RMT in Section III-A, followed by the derivation for the densities for all  $\beta$  in Sections III-B–III-D.

### A. Background

For the density  $\hat{p}(\lambda) : \mathbb{R} \rightarrow \mathbb{R}$ , its Stieltjes transform  $\hat{s} = \hat{s}(z)$  is a complex valued function defined as

$$\hat{s}(z) = \int_{-\infty}^{\infty} \frac{\hat{p}(\lambda)}{\lambda - z} d\lambda, \quad z \in \mathbb{C}^+ = \{z \in \mathbb{C} | \text{Im}[z] > 0\}. \quad (27)$$

Equation (27) can be inverted explicitly to retrieve the density as [13]

$$\hat{p}(\lambda) = \lim_{\epsilon \rightarrow 0^+} \frac{1}{\pi} \text{Im}[\hat{s}(\lambda + i\epsilon)]. \quad (28)$$

Since for all  $\beta \in (0, \infty)$ ,  $\Sigma$  is bounded in spectral norm and the observations follow Gaussian statistics in (5), the Stieltjes transform  $\hat{s}$  of the asymptotic eigenvalue density  $\hat{p}(\lambda)$  is a solution to [30]

$$\hat{s} = \sum_{i=1,2} \frac{\xi_i}{\Lambda_i(1 - \nu - \nu z \hat{s}) - z}. \quad (29)$$

As  $\nu \rightarrow 0$ ,  $\hat{s} \rightarrow s$ , which is the Stieltjes transform of  $p(\lambda)$ , the eigenvalue density of  $\Sigma$  in (20), and is given by

$$s = \sum_{i=1,2} \frac{\xi_i}{\Lambda_i - z}. \quad (30)$$

Considering (29) for  $z \rightarrow \lambda \in \mathbb{R} \setminus \{0\}$  and simplifying,  $\hat{s}$  then is the root of a polynomial with real coefficients (whose degree is 2 or 3, depending on the number of distinct nonzero eigenvalues of  $\Sigma$ ). Since the array element spacing, frequency of interest and the ratio of number of array elements to the number of snapshots are known, (29) can be solved in terms of  $\beta$  (or equivalently,  $\Lambda_i$  and  $\xi_i$ ) and  $\nu$ .

Since  $\hat{p}(\lambda)$  has not been defined at  $\lambda = 0$ , we define it as follows, using the fact that the area under the density is 1:

$$\hat{p}(0) = 1 - \int_{\lambda > 0} \hat{p}(\lambda) d\lambda. \quad (31)$$

Noting that covariance matrices are nonnegative definite (i.e., eigenvalues are nonnegative) and that the normalized ranks  $\mathcal{R}(\Sigma)$  and  $\mathcal{R}(\hat{\Sigma})$  are equal in the asymptotic limit, it follows that:

$$\hat{p}(0) = p(0) = \begin{cases} \xi_2 & \beta < \frac{1}{2} \\ 0 & \text{otherwise.} \end{cases} \quad (32)$$

### B. Density for Spatially Oversampled Case ( $\beta < \frac{1}{2}$ )

In this section, the eigenvalue density is first derived from the MP density using linear algebra and then again using Stieltjes transforms in order to illustrate concepts essential in Section III-D.

Using the eigendecomposition  $\Sigma = \mathbf{U}\mathbf{\Lambda}\mathbf{U}^H$  in (5) gives

$$\hat{\Sigma} = \frac{1}{M} \mathbf{U} \mathbf{\Lambda}^{\frac{1}{2}} \mathbf{X}' \left( \mathbf{\Lambda}^{\frac{1}{2}} \mathbf{X}' \right)^H \mathbf{U}^H \quad (33)$$

where  $\mathbf{X}'$  is also an  $N \times M$  random matrix with elements  $\sim \mathcal{CN}(0, 1)$  (since  $\mathbf{X}$  is GUE). From (22), the eigenvalues of  $\Sigma$  and  $\mathbf{\Lambda}$  are  $\Lambda_1$  with multiplicity ratio  $\xi_1$  and zero with multiplicity ratio  $\xi_2$ . Due to the zero eigenvalue, only the upper  $\xi_1$  portion of  $\mathbf{X}'$  contributes to the matrix multiplication in the asymptotic limit or equivalently, the array elements to snapshot ratio decreases to  $\tilde{\nu} = \nu \xi_1$ . Hence the distribution of the nonzero eigenvalue of  $\hat{\Sigma}$  also follows the MP density in (6), albeit with  $\tilde{\nu}$  instead of  $\nu$ .

So, the eigenvalue density of  $\hat{\Sigma}$  can be written as

$$\hat{p}(\lambda) = \begin{cases} \xi_1 \frac{\sqrt{(\lambda_+ - \lambda)(\lambda - \lambda_-)}}{2\pi\nu\lambda} & \lambda_- < \lambda < \lambda_+ \\ \xi_2 \delta(\lambda) & \text{otherwise.} \end{cases} \quad (34)$$

Here,  $\lambda_{\pm}$  are modified forms of  $l_{\pm}$  in (6), to account for  $\tilde{\nu}$  and the scaling by  $\Lambda_1$ , given by

$$\lambda_{\pm} = \Lambda_1 (1 \pm \sqrt{\tilde{\nu}})^2 = \frac{(1 + \sqrt{2\beta\nu})^2}{2\beta}. \quad (35)$$

The first term in (34) accounts for the density due to the spreading of the nonzero eigenvalue  $\Lambda_1$  [see Fig. 3(a)] and the second term in (34) is the density due to the zero eigenvalue. The density at  $\lambda = 0$  remains unchanged from that of the true CM as in (32). Note that although the first term is similar in form to the M-P density in (6), the spreading  $\lambda_{\pm}$  is different and is given by (39).

Equation (34) also can be arrived at using the Stieltjes transform in Section III-A. Using  $\Lambda_i$  and  $\xi_i$  from (22) and (23), (29) simplifies to

$$\nu\lambda^2 \hat{s}^2 + \lambda [2\beta\lambda - 2(\beta - 1)\nu - 1] \hat{s} + 2\beta(1 - \nu + \lambda) + \nu - 1 = 0. \quad (36)$$

To obtain the density  $\hat{p}$  from (28), (36) is solved for  $\hat{s}$ , keeping only the solution where  $\text{Im}[\hat{s}] > 0$  since  $\hat{p}(\lambda) > 0$ , resulting in

$$\text{Im}[\hat{s}] = \frac{\sqrt{-D}}{(2\nu\lambda^2)} \quad \text{for } D < 0 \quad (37)$$

where the discriminant  $D$  is factored as

$$D = \lambda^2 [4\beta^2(\nu - \lambda)^2 - 4\beta(\nu + \lambda) + 1] = 4\beta^2 \lambda^2 (\lambda - \lambda_-)(\lambda - \lambda_+) \quad (38)$$

with

$$\lambda_{\pm} = \frac{(1 \pm \sqrt{2\beta\nu})^2}{2\beta} = (\sqrt{\Lambda_1} \pm \sqrt{\nu})^2 \quad (39)$$

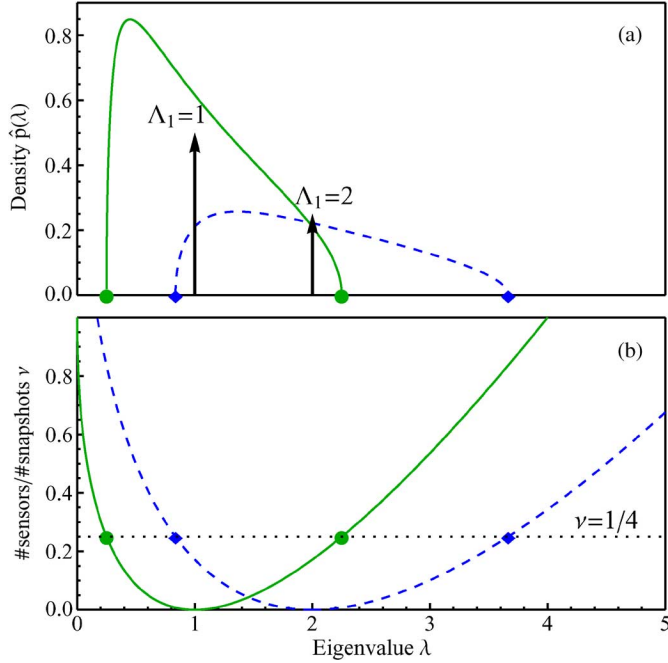


Fig. 3. (a) Asymptotic eigenvalue density for  $\nu = \frac{1}{4}$  and  $\beta = \frac{1}{4}$  (dashed,  $\Lambda_1 = 2$ ) and  $\beta = \frac{1}{2}$  (solid, M-P density,  $\Lambda_1 = 1$ ). Only the contribution from the nonzero eigenvalue is shown for  $\beta = \frac{1}{4}$ . The extent of spreading is marked by symbols and the nonzero eigenvalue  $\Lambda_1$  in each case is marked by an arrow. (b) Change in the spreading of the densities in (a) for different  $\nu$ .

which is identical to (35). Hence, the real roots of the discriminant  $D$  provide the bounds for the density.  $\text{Im}[\hat{s}]$  can then be written as

$$\text{Im}[\hat{s}] = \begin{cases} \frac{\xi_1 \sqrt{(\lambda_+ - \lambda)(\lambda - \lambda_-)}}{2\nu\lambda} & \lambda_- < \lambda < \lambda_+, \\ 0 & \text{otherwise} \end{cases} \quad (40)$$

and from (28) and (32), (34) can be obtained.

Typically, in array processing applications, zero eigenvalues are encountered only when the SCM is snapshot starved ( $\nu > 1$ ). However, from (34), the SCM always will be degenerate for  $\beta < \frac{1}{2}$ .

#### C. Density for Spatially Nyquist Sampled Case ( $\beta = \frac{1}{2}$ )

The density in this case and for all  $\beta = \frac{q}{2}$ ,  $q \in \mathbb{N}$  is given by the M-P density as discussed in Section I-B. Equation (34) is a generalized form of M-P and indeed (6) follows from (34) for  $\Lambda_1 = 1$  and  $\xi_2 = 0$ . From Fig. 3(b), it is clear that the spreading of the eigenvalues is wider in the oversampled case (dashed) than the Nyquist sampled case (solid), even though the noise power on each sensor is the same.

#### D. Density for Spatially Undersampled Case ( $\beta > \frac{1}{2}$ )

Eigenvalue densities for SCMs, where the true CM has two nonzero eigenvalues (with multiplicities), have been studied in the context of detecting signals in uncorrelated noise [32]. Proceeding as in the previous section, (29) simplifies to

$$\begin{aligned} & \hat{s}^3 \lambda^2 \Lambda_1 \Lambda_2 \nu^2 + \hat{s}^2 \lambda \nu [\lambda(\Lambda_1 + \Lambda_2) + 2\Lambda_1 \Lambda_2 (\nu - 1)] \\ & + \hat{s} [\lambda^2 + \lambda \nu (\Lambda_2 \xi_1 + \Lambda_1 \xi_2) + \lambda(\Lambda_1 + \Lambda_2)(\nu - 1) \\ & + \Lambda_1 \Lambda_2 (\nu - 1)^2] + \lambda + (\Lambda_1 \xi_2 + \Lambda_2 \xi_1)(\nu - 1) = 0. \end{aligned} \quad (41)$$

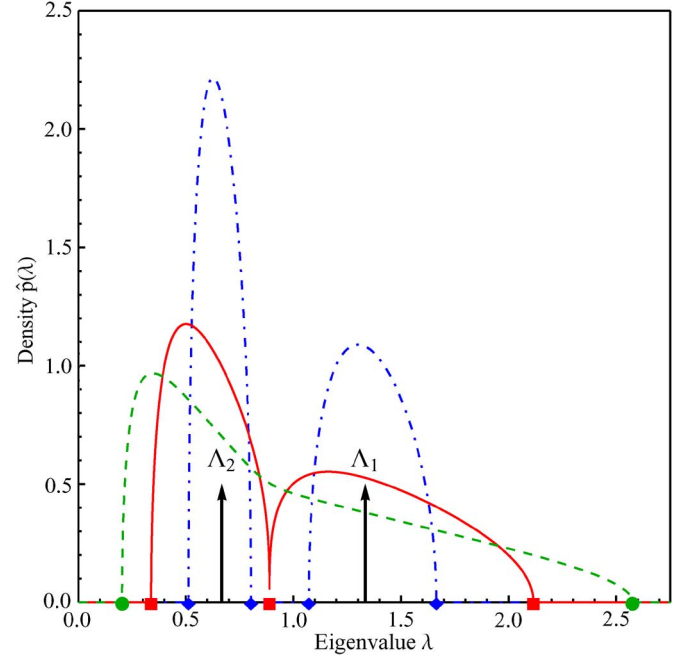


Fig. 4. Asymptotic eigenvalue density of the SCM for  $\beta = \frac{3}{4}$  and  $\nu = \frac{1}{40}$  (dot-dashed),  $\nu = \frac{1}{4}$  (dashed) and  $\nu_s \approx 0.115$  the value of  $\nu$  where the two regions combine (dotted). Each of these densities have finite intervals, marked by symbols. The eigenvalues  $\Lambda_1$  and  $\Lambda_2$  of the true CM  $\Sigma$  are shown by the arrows.

The above cubic has one real root and the other two roots, if complex, exist as conjugate pairs. Normalizing (41) to the form  $\hat{s}^3 + a_2 \hat{s}^2 + a_1 \hat{s} + a_0 = 0$ , the desired solution for  $\text{Im}[\hat{s}]$  is given by

$$\text{Im}[\hat{s}] = \text{Im} \left[ \frac{(1 + i\sqrt{3})R}{2} + \frac{(1 - i\sqrt{3})Q}{2R} \right] \quad (42)$$

where  $R = \sqrt[3]{P + \sqrt{-D}}$  and  $Q = \frac{(a_2^3 - 3a_1)}{9}$ , with the discriminant  $D = Q^3 - P^2$  and  $P = \frac{(-2a_2^3 + 9a_1 a_2 - 27a_0)}{54}$ . Finally, to obtain the density from (28),  $\text{Im}[\hat{s}]$  is replaced with  $|\text{Im}[\hat{s}]|$  to include the positive contribution from the conjugate solution (see Fig. 4).

As in the previous section the real roots of the discriminant  $D$  (considering it as a polynomial in  $\lambda$ ) give the bounds where  $\hat{p}(\lambda) > 0$ . The spreading of the eigenvalue density [Fig. 5(a)] can be understood from a physical viewpoint as follows.

When the SCM  $\hat{\Sigma}$  is formed from a relatively smaller number of snapshots, i.e.,  $M \sim N$  or  $\nu \sim 1$ , there is a larger uncertainty as to what the true eigenvalues are (small sample size). This results in the eigenvalues of the SCM spreading across the two true eigenvalues and resulting in a single spread out region [dashed line in Fig. 4 and Fig. 5(a)].

When the number of snapshots is much larger than the number of array elements i.e.,  $\nu \ll 1$ , the uncertainty in the sample eigenvalues reduces and there are two intervals where  $\hat{p}(\lambda) > 0$ , localized around each of the true eigenvalues [dot-dashed line in Fig. 4 and Fig. 5(a)]. Having two distinct intervals is equivalent to the discriminant having four real roots.

The presence of two lobes in the eigenvalue density of the SCM has implications in signal detection. For example, if one

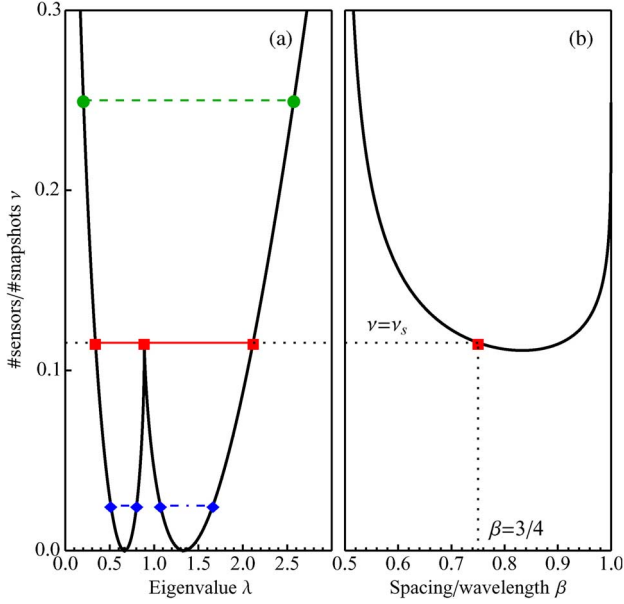


Fig. 5. (a) Spreading of the asymptotic eigenvalue density for  $\beta = \frac{3}{4}$ , showing the intervals of supports for  $\nu = \frac{1}{4}$  (dashed, circles),  $\nu = \frac{1}{40}$  (dot-dashed, diamonds) and  $\nu = \nu_s \approx 0.115$  (horizontal solid line, squares) where the density splits into two intervals. (b) Change in  $\nu_s$  with  $\beta$  for  $\beta \in (\frac{1}{2}, 1)$  and the solid square marks  $\nu_s$  corresponding to  $\beta = \frac{3}{4}$  in (b).

were unaware of this phenomenon, one might conclude erroneously that the lobe associated with the larger eigenvalue is due to a signal, when in reality, it is only noise. Therefore, it is of interest to determine at what value of  $\nu$  the density splits in two so as to take into account when processing data.

In Fig. 5(a), the curve splits into two distinct lobes at  $\nu \approx 0.115$ . The  $\nu$  where this occurs,  $\nu_s$  is a double root and can be obtained by setting the discriminant of the discriminant of the cubic to zero (see Appendix), and is found as

$$\nu_s = \frac{(\Lambda_1 - \Lambda_2)^2}{\left[ (\Lambda_1^2 \xi_1)^{\frac{1}{3}} + (\Lambda_2^2 \xi_2)^{\frac{1}{3}} \right]^3}. \quad (43)$$

The resulting curve for  $\nu_s$  for  $\beta \in (\frac{1}{2}, 1)$  is shown in Fig. 5(b). At all values of  $\nu$  below this curve, the density will have two lobes.

#### IV. EIGENVALUE DENSITY OF THE SCM FOR FINITE $N$

Matrices of the type  $\mathbf{X}\mathbf{X}^H$ , where  $\mathbf{X}$  is a GUE random matrix, are known as Wishart matrices [33] and the joint probability densities of their eigenvalues have been known for a while [34]–[37]. These densities are generally expressed as hypergeometric functions of the matrices themselves and are complicated and difficult to work with for both numerical and analytical analysis [37]. In recent work, the form of these expressions were simplified by rederiving in terms of the product of two determinants [38], [39].

The results from [39] are applied to the isotropic noise SCM and the corresponding densities for different  $\beta$  are given in (44) and (45) in Appendix B. In Fig. 6 the analytical densities for  $N = 20$  (solid line) and the asymptotic density (dashed line) are shown for different values of  $\beta$ . The simpler asymptotic solution

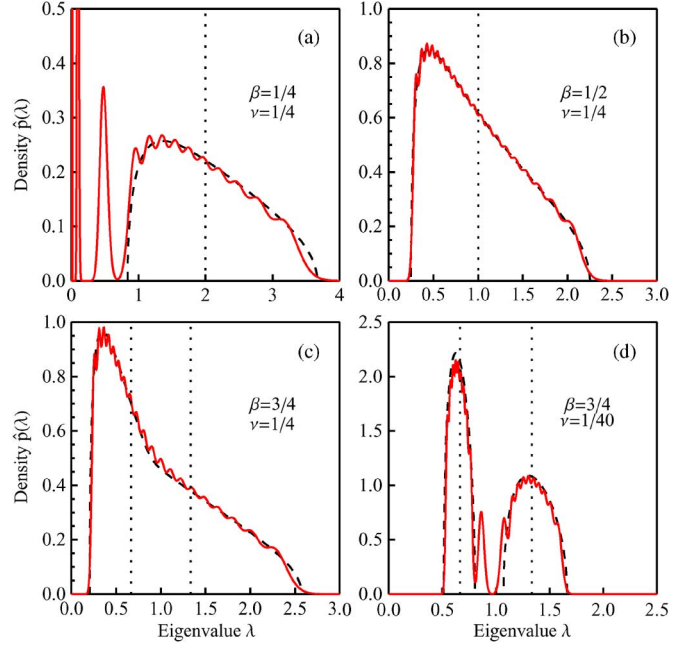


Fig. 6. Asymptotic eigenvalue density (dashed line) and the analytical density for finite  $N$ , with  $N = 20$  array elements, and (a–c) spacing to wavelength ratios  $\beta = \frac{1}{4}$ ,  $\frac{1}{2}$ , and  $\frac{3}{4}$ , respectively, for  $\nu = \frac{1}{4}$  (ratio of number of sensors to number of snapshots) i.e.  $M = 80$  and (d)  $\beta = \frac{3}{4}$  for  $\nu = \frac{1}{40}$ , i.e.,  $M = 800$ .

holds well for modest values of  $N$ , although it does not capture the effect of the transition eigenvalues [Fig. 6 in panel (a) around 0.5 and panel (d) around 0.8]. The number of local peaks in the solid line is the same as the number of distinct eigenvalues of the finite SCM, and correspond to the expectation of the means of the individual eigenvalues.

Evaluation of (44) and (45) are computationally intensive even for modest  $N$ . The computational complexity increases drastically with  $N$  [roughly  $\mathcal{O}(N^4)$ ], and the large exponents of both large and small numbers in the expressions make it unsuitable for numerical work without significant effort due to the limitations of floating point arithmetic. This is not immediately apparent from [39], as only the  $N = 3$  case is considered there. In comparison, the asymptotic result captures most of the features of the eigenvalue density, and can be easily calculated from (34) or (42).

#### V. SIMULATIONS

A Monte Carlo simulation is performed to compare the theoretical asymptotic results with the empirical eigenvalue density obtained for a finite  $N$ . In Fig. 7 and Fig. 8, realizations of the SCM are obtained as in (5) and the empirical densities of the eigenvalues are averaged over 1000 realizations in order to obtain statistically stable distributions. The asymptotic solution (solid lines) are obtained from (34) for  $\beta = \frac{1}{4}$ , (6) for  $\beta = \frac{1}{2}$  and (28) with (42) for  $\beta = \frac{3}{4}$ .

Fig. 7 shows the resulting empirical densities when  $\nu = \frac{1}{4}$  and different  $\beta$  for  $N = 100$  [Fig. 7(a)–(c)] and  $N = 20$  [Fig. 7(d)–(f)], respectively. In Fig. 7(a), nearly half the area is due to the peak at  $\lambda = 0$  [exactly half in the asymptotic limit, as  $\hat{p}(0) = \xi_2 = \frac{1}{2}$  from (32)]. The asymptotic solutions describe the empirical densities quite well, except for tails at large  $\lambda$  as

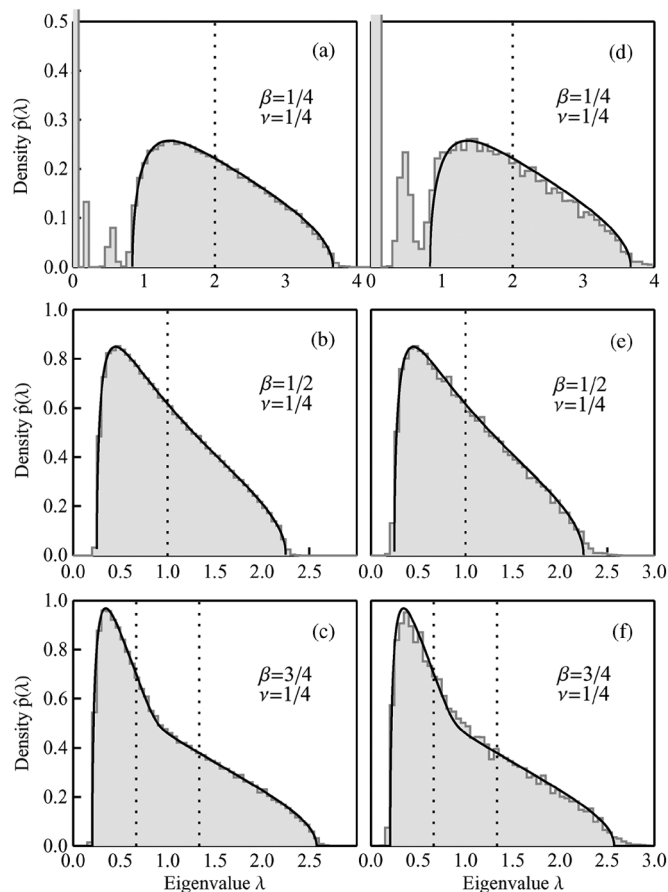


Fig. 7. Asymptotic eigenvalue density (solid line) and the empirical eigenvalue density (gray), with  $N = 100$  array elements,  $\nu = \frac{1}{4}$  (ratio of number of sensors to number of snapshots) and spacing to wavelength ratios  $\beta$  of (a)  $1/4$ . (b)  $1/2$ . (c)  $3/4$ . (d), (e), (f) Same as in (a, b, c) except with  $N = 20$ . The dotted lines show the locations of the distinct nonzero true eigenvalues. In (a) and (d), the  $y$  axis is only shown between 0–0.5 so as to display the density due to the nonzero eigenvalue prominently.

opposed to a sharp edge in the asymptotic case, which become more prominent as  $N$  decreases [e.g., Fig. 7(b) vs Fig. 7(e)].

Another clear consequence of finite  $N$ , is the contribution from transition eigenvalues, seen between 0.1–0.8 in Fig. 7(a), (d) for  $\beta = \frac{1}{4}$ . While their effect is not seen in Fig. 7(c), (f) at  $\nu = \frac{1}{4}$  for  $\beta = \frac{3}{4}$ , it becomes apparent when the number of snapshots is increased to  $\nu = \frac{1}{40}$  in Fig. 8(c), (f). Here, the densities localize around the two asymptotic eigenvalues ( $\Lambda_1 = \frac{4}{3}$  and  $\Lambda_2 = \frac{2}{3}$ ) and the contributions from the transition eigenvalues [centered around  $\frac{n}{N} = \xi_1 = 0.5$  in Fig. 8(a), (d), where  $\xi_1$  is from (25)] fill up the region in between them. Even at  $\nu = \nu_s \approx 0.115$ , when the density splits in the asymptotic case, the empirical density does not split entirely because of the transition eigenvalues, resulting in a nonzero contribution in Fig. 8(b), (e).

Both of the above effects (tails and contributions from transition eigenvalues) are due to the finite dimension of the SCM and hence, they are not present in the asymptotic result. These effects become more pronounced as  $N$  decreases, because the transition eigenvalues form a larger percentage of the total number of eigenvalues [6/20 in Fig. 8(d) vs. 6/100 in Fig. 8(a)]. The difference between the largest eigenvalue of the CM in

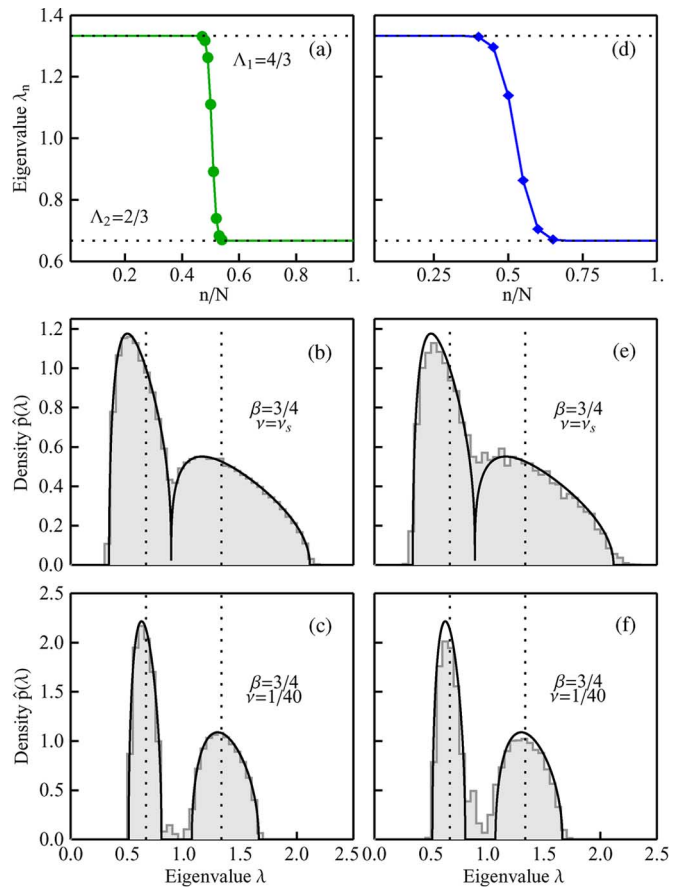


Fig. 8. Effect of transition eigenvalues on the empirical eigenvalue density (gray) for  $\beta = \frac{3}{4}$  and (a)–(c)  $N = 100$  and (d)–(f)  $N = 20$ . (a) and (d) Eigenvalues of the CM. The  $x$  axis is a normalized index where  $n = \{1, \dots, N\}$ . Only eigenvalues deviating from either  $\Lambda_1$  or  $\Lambda_2$  by 0.1% are marked. (b) and (e) Empirical density of the SCM  $\nu = \nu_s \approx 0.115$  when the density splits. (c) and (f) Same as (b) and (e) for  $\nu = \frac{1}{40}$ . The asymptotic density is shown by the solid line.

Fig. 8(a), (d) and the corresponding asymptotic value in (24) is on the order of  $10^{-14}$  for  $N = 20$  and  $10^{-15}$  for  $N = 100$ , indicating that the analytical solution is quite accurate.

## VI. CONCLUSION

In this paper, the asymptotic eigenvalue densities have been derived for noise covariance matrices (CM) for line arrays with uniformly spaced elements in an isotropic noise field. The CM has at most two distinct eigenvalues for all values of  $\beta$ , the ratio of interelement spacing to wavelength. From independent observations of the noise field, a sample noise covariance matrix (SCM) is formed using more snapshots than the number of array elements and its eigenvalues are analyzed using random matrix theory (RMT).

When the sensors are spaced less than half a wavelength apart, the SCM is always singular, no matter how many snapshots are used. For spacings of more than half a wavelength apart, the SCM is full rank if sufficient snapshots are used, but the eigenvalue density can split into two distinct densities.

Analytical results for finite Wishart matrices and simulations with finite SCMs confirm the asymptotic results derived using RMT. The results hold well even for arrays with as low as 20 sensors.

## APPENDIX A

OUTLINE OF APPROACH TO SOLVE FOR  $\nu_s$ 

The derivation of (43) is tedious and the intermediate equations are lengthy and hence, omitted. An outline of the approach is provided here with hints.

- 1) Starting with (41), calculate the discriminant of the polynomial in  $\hat{s}$ . The result is a polynomial of degree 8 in  $\lambda$  that can be factored into a product of  $\lambda^4$  and a quartic in  $\lambda$ .
- 2) Noting that  $\lambda > 0$ , only the quartic needs to be considered. Calculating the discriminant of the quartic results in a polynomial of degree 23 in  $\nu$ , which can be factored into a product of  $\nu^{14}$  and a polynomial of degree 9 in  $\nu$ .
- 3) Again, discarding the  $\nu^{14}$  term, the remaining degree 9 polynomial can be simplified into a cube of a cubic in  $\nu$ . Finally,  $\nu_s$  is the real root of

$$\begin{aligned} & \nu^3 (\Lambda_1^2 \xi_1 + \Lambda_2^2 \xi_2)^3 \\ & - 3\nu^2 (\Lambda_1 - \Lambda_2)^2 (\Lambda_1^4 \xi_1^2 - 7\Lambda_2^2 \Lambda_1^2 \xi_1 \xi_2 + \Lambda_2^4 \xi_2^2) \\ & + 3\nu (\Lambda_1 - \Lambda_2)^4 (\Lambda_1^2 \xi_1 + \Lambda_2^2 \xi_2) - (\Lambda_1 - \Lambda_2)^6 = 0 \end{aligned}$$

which upon simplifying, gives (43).

## APPENDIX B

EIGENVALUE DENSITY OF THE SCM FOR FINITE  $N$ 

Let  $\Sigma_N$  and  $\hat{\Sigma}_N$  denote the isotropic noise CM and SCM when  $N$  is finite and  $\sigma_1, \dots, \sigma_N$  be the eigenvalues of  $\Sigma_N$ . The following expressions are adapted from [39], using the notation followed in this text where necessary.

A. Density When  $\beta = \frac{q}{2}$ ,  $q \in \mathbb{N}$ 

Using (38) in [39], the density for finite  $N$  when  $\beta = \frac{q}{2}$ ,  $q \in \mathbb{N}$  (i.e.,  $\Sigma$  is the identity matrix) is

$$\hat{p}_N(\lambda) = K \sum_{n=1}^N \sum_{n'=1}^N (-1)^{n+n'} (M\lambda)^{n+n'-2+M-N} \times e^{-M\lambda} \det(\Omega(n, n')) \quad (44)$$

where

$$\begin{aligned} K &= \frac{M}{\prod_{i=1}^N (M-i)! \prod_{j=1}^N (N-j)!} \\ \Omega_{ij}(n, n') &= N^{\frac{-1}{(N-1)}} [\mu_{ij}(n, n') + M - N]! \\ \mu_{ij}(n, n') &= \begin{cases} i+j-2 & \text{if } i < n \text{ and } j < n' \\ i+j & \text{if } i \geq n \text{ and } j \geq n' \\ i+j-1 & \text{otherwise} \end{cases} \end{aligned}$$

B. Density for all Other  $\beta$ 

Using (41) in [39], the density for all other  $\beta$  for finite  $N$  is

$$\hat{p}_N(\lambda) = K' \sum_{n=1}^N \sum_{n'=1}^N (-1)^{n+n'} (M\lambda)^{M-N+n-1} \times e^{\frac{-M\lambda}{\sigma_{n'}}} \det(\Omega'(n, n')) \quad (45)$$

where

$$\begin{aligned} K' &= K \prod_{i=1}^N (i-1)! \frac{\det(\Sigma_N)^{-M}}{\det(\mathbf{V})} \\ \mathbf{V}_{ij} &= (-\sigma_j)^{1-i} \\ \Omega'_{ij}(n, n') &= N^{\frac{-1}{(N-1)}} (\sigma_{r(j, n')})^{M-N+r(i, n)} \\ &\quad \times (M - N + r(i, n) - 1)! \\ r(i, j) &= \begin{cases} i & i < 0j \\ i+1 & i \geq j. \end{cases} \end{aligned}$$

## REFERENCES

- [1] O. I. Lobkis and R. L. Weaver, "On the emergence of the Green's function in the correlations of a diffuse field," *J. Acoust. Soc. Amer.*, vol. 110, pp. 3011–3017, Dec. 2001.
- [2] R. L. Weaver and O. I. Lobkis, "Ultrasonics without a source: Thermal fluctuation correlations at MHz frequencies," *Phys. Rev. Lett.*, vol. 87, p. 134301, 2001.
- [3] K. G. Sabra, P. Gerstoft, P. Roux, W. A. Kuperman, and M. C. Fehler, "Extracting time-domain Green's function estimates from ambient seismic noise," *Geophys. Res. Lett.*, vol. 32, p. L03310, 2005.
- [4] N. M. Shapiro, M. Campillo, L. Stehly, and M. H. Ritzwoller, "High-resolution surface-wave tomography from ambient seismic noise," *Sci.*, vol. 307, pp. 1615–1618, 2005.
- [5] P. Roux and W. A. Kuperman, NPAL group, "Extracting coherent wave fronts from acoustic ambient noise in the ocean," *J. Acoust. Soc. Amer.*, vol. 116, pp. 1995–2003, 2004.
- [6] L. A. Brooks and P. Gerstoft, "Green's function approximation from cross-correlations of 20–100 Hz noise during a tropical storm," *J. Acoust. Soc. Amer.*, vol. 125, pp. 723–734, Jan 2009.
- [7] A. Duroux, K. G. Sabra, J. Ayers, and M. Ruzzane, "Extracting guided waves from cross-correlations of elastic diffuse fields: Applications to remote structural health monitoring," *J. Acoust. Soc. Amer.*, vol. 127, pp. EL42–EL47, 2010.
- [8] M. L. Mehta, *Random Matrices*, 3rd ed. New York: Academic, 2004.
- [9] A. Edelman and N. R. Rao, "Random matrix theory," *Acta Numerica*, vol. 14, no. 1, pp. 233–297, 2005.
- [10] H. Cox, "Spatial correlation in arbitrary noise fields with application to ambient sea noise," *J. Acoust. Soc. Amer.*, vol. 54, no. 5, pp. 1289–1301, 1973.
- [11] R. R. Nadakuditi and A. Edelman, "Sample eigenvalue based detection of high-dimensional signals in white noise using relatively few samples," *IEEE Trans. Signal Process.*, vol. 56, no. 7, pp. 2625–2638, 2008.
- [12] R. R. Müller, "A random matrix model of communication via antenna arrays," *IEEE Trans. Inf. Theory*, vol. 48, no. 9, pp. 2495–2506, 2002.
- [13] A. M. Tulino and S. Verdú, "Random matrix theory and wireless communications," *Found. Trends in Commun. Inf. Theory*, vol. 1, no. 1, pp. 1–182, 2004.
- [14] R. L. Weaver, "Spectral statistics in elastodynamics," *J. Acoust. Soc. Amer.*, vol. 85, pp. 1005–1013, 1989.
- [15] A. Aubry and A. Derode, "Random matrix theory applied to acoustic backscattering and imaging in complex media," *Phys. Rev. Lett.*, vol. 102, p. 084301, 2009.
- [16] A. Aubry and A. Derode, "Detection and imaging in a random medium: A matrix method to overcome multiple scattering and aberration," *J. Appl. Phys.*, vol. 106, p. 044903, 2009.
- [17] S. E. Skipetrov and A. Goetschy, "Eigenvalue distributions of large Euclidean random matrices for waves in random media," *J. Phys. A: Math. Theor.*, vol. 44, p. 065102, 2011.
- [18] X. Mestre, "On the asymptotic behavior of the sample estimates of eigenvalues and eigenvectors of covariance matrices," *IEEE Trans. Signal Process.*, vol. 56, no. 11, pp. 5353–5368, 2008.
- [19] R. R. Nadakuditi and J. W. Silverstein, "Fundamental limit of sample generalized eigenvalue based detection of signals in noise using relatively few signal-bearing and noise-only samples," *IEEE J. Sel. Topics in Signal Process.*, vol. 4, no. 3, pp. 468–480, 2010.
- [20] V. A. Marčenko and L. A. Pastur, "Distributions of eigenvalues of some sets of random matrices," *Math. Sb.*, vol. 72, pp. 507–536, 1967.

- [21] D. Slepian, "Prolate spheroidal wave functions, Fourier analysis, and uncertainty—V: The discrete case," *Bell Syst. Tech. J.*, vol. 57, no. 5, pp. 1371–1430, 1978.
- [22] M. Zatman, "Production of adaptive array troughs by dispersion synthesis," *Electron. Lett.*, vol. 31, no. 25, pp. 2141–2142, 1995.
- [23] R. J. Mailloux, "Covariance matrix augmentation to produce adaptive array pattern troughs," *Electron. Lett.*, vol. 31, no. 25, pp. 771–772, 1995.
- [24] U. Grenander and G. Szegő, *Toeplitz Forms and Their Applications*. New York: Chelsea, 1984.
- [25] R. M. Gray, "Toeplitz and circulant matrices: A review," *Found. Trends. Commun. Inf. Theory*, vol. 2, no. 3, pp. 155–239, 2006.
- [26] H. J. Landau and H. Widom, "The eigenvalue distribution and frequency limiting," *J. Math. Anal.*, vol. 77, pp. 469–481, 1980.
- [27] D. Slepian, "Some comments on Fourier analysis, uncertainty and modeling," *SIAM Rev.*, vol. 25, no. 3, pp. 379–393, 1983.
- [28] L. Cottatellucci, R. R. Müller, and M. Debbah, "Asynchronous CDMA systems with random spreading—Part I: Fundamental limits," *IEEE Trans. Inf. Theory*, vol. 56, no. 4, pp. 1477–1497, 2010.
- [29] D. H. Johnson and D. E. Dudgeon, *Array Processing: Concepts and Techniques*. Englewood Cliffs, NJ: Prentice-Hall, 1993.
- [30] J. W. Silverstein, "Strong convergence of the empirical distribution of eigenvalues of large dimensional random matrices," *J. Multivar. Anal.*, vol. 54, pp. 175–192, 1995.
- [31] J. W. Silverstein and S. Choi, "Analysis of the limiting spectral distribution of large dimensional random matrices," *J. Multivar. Anal.*, vol. 54, pp. 395–209, 1995.
- [32] Z. Burda, A. T. Görlich, A. Jarosz, and J. Jurkiewicz, "Signal and noise in correlation matrix," *Physica A*, vol. 343, pp. 295–310, 2004.
- [33] J. Wishart, "The generalized product moment distribution in samples from a normal multivariate population," *Biometrika*, vol. 20A, pp. 32–52, 1928.
- [34] A. T. James, "The distribution of the latent roots of the covariance matrix," *Ann. Math. Statist.*, vol. 31, pp. 151–158, 1960.
- [35] T. W. Anderson, "Asymptotic theory for principal component analysis," *Ann. Statist.*, vol. 34, pp. 122–148, 1963.
- [36] T. W. Anderson, *An Introduction to Multivariate Statistical Analysis*, 2nd ed. New York: Wiley, 1984.
- [37] M. Siotani, T. Hayakawa, and Y. Fujikoshi, *Modern Multivariate Statistical Analysis: A Graduate Course and Handbook*. New York: American Sciences, 1985.
- [38] M. Chiani, M. Z. Win, and A. Zanella, "On the capacity of spatially correlated MIMO Rayleigh fading channels," *IEEE Trans. Inf. Theory*, vol. 49, no. 10, pp. 2363–2371, 2003.
- [39] A. Zanella, M. Chiani, and M. Z. Win, "On the marginal distribution of the eigenvalues of Wishart matrices," *IEEE Trans. Commun.*, vol. 57, no. 4, pp. 1050–1060, 2009.



and statistical learning, with applications in acoustical oceanography and seismology.



Dr. Gerstoft is a Fellow of the Acoustical Society of America and an elected member of the International Union of Radio Science, Commission F.



sensor networks, propagation modeling, ambient noise, and environmental inversions, with applications of these to underwater acoustics and electromagnetic wave propagation.

Dr. Hodgkiss is a Fellow of the Acoustical Society of America.

**Ravishankar Menon** (S'12) received the B.Tech. and M.Tech. degrees in naval architecture and ocean engineering, with a minor in operations research, from the Indian Institute of Technology Madras, in 2008, and the M.S. degree in oceanography from the Scripps Institution of Oceanography, University of California San Diego (UCSD), La Jolla, in 2010.

He is currently a Ph.D. candidate in the Department of Electrical and Computer Engineering, UCSD. His research interests include signal processing, remote sensing with ambient noise, with applications in acoustical oceanography and

**Peter Gerstoft** received the Ph.D. degree from the Technical University of Denmark, Lyngby, Denmark, in 1986.

From 1992 to 1997, he was with Nato Undersea Research Centre, La Spezia, Italy. Since 1997, he has been with the Marine Physical Laboratory, University of California, San Diego. His research interests include modeling and inversion of acoustic, elastic, and electromagnetic signals.

Dr. Gerstoft is a Fellow of the Acoustical Society of America and an elected member of the International Union of Radio Science, Commission F.

**William S. Hodgkiss** (S'68–M'75) received the Ph.D. degree in electrical engineering from Duke University, Raleigh, NC, in 1975.

Since 1978, he has been a member of the faculty of the Scripps Institution of Oceanography, University of California, San Diego, and on the staff of the Marine Physical Laboratory where currently he is Deputy Director. He also serves as Associate Vice Chancellor for Academic Personnel and Resources at UCSD. His present research interests are in the areas of signal processing, communications, wireless